AFRL-SR-AR-TR-08-0180

REPORT DOCUMENTATION PAGE

1. AGENCY USE ONLY (Leave blank)	2. REPORT DATE 02/026/2008	3. REPORT TYPE AND DATES COVERED Final Performance Report, 03/01/05-12/31/07

4. TITLE AND SUBTITLE
Computational Study of Separation Control Using ZNMF Devices: Flow Physics and Scaling Laws

5. FUNDING NUMBERS
FA9550-05-1-0169

6. AUTHOR(S)
Rajat Mittal, PhD

7. PERFORMING ORGANIZATION NAME(S) AND ADDRESS(ES)
The George Washington University
801 22nd St. NW
Washington DC 20052

8. PERFORMING ORGANIZATION REPORT NUMBER

9. SPONSORING / MONITORING AGENCY NAME(S) AND ADDRESS(ES)
AFOSR
4015 Wilson Boulevard
Room 713
Arlington VA 22203-1954
Brett Jeffries/NA

10. SPONSORING / MONITORING AGENCY REPORT NUMBER

11. SUPPLEMENTARY NOTES

12a. DISTRIBUTION / AVAILABILITY STATEMENT
Approved for public release; distribution unlimited.

12b. DISTRIBUTION CODE

13. ABSTRACT ***(Maximum 200 Words)***

The primary objective of the proposed research was to gain a fundamental understanding of strategies, mechanisms, and scaling laws for successful control of separation using zero-net mass-flux (ZNMF) actuators. The key issue that was systematically studied was the optimal excitation frequencies in separated flows characterized by convective and/or global instabilities. The study was a complementary experimental/numerical effort that capitalized on previous collaborations and was aimed at leveraging the respective strengths of CFD and experiments. The numerical component employed two different solvers will allowed us to investigate chord Reynolds numbers Re_c up to $O(10^5)$. The complementary experiments use a large flat plate model equipped with a two-dimensional ZNMF actuator slot. Both the experiments and computations employed nonlinear spectral analysis to quantify quadratic coupling between the various instability mechanisms in separated flows. Outcomes included fundamental insights into the non-linear dynamics of separated airfoil flows and their implications for ZNMF separation control as well as development of improved lumped element design tool for ZNMF actuators in separation control applications.

14. SUBJECT TERMS
Flow Control, Synthetic jets, Computational Fluid Dynamics

15. NUMBER OF PAGES
14

16. PRICE CODE

17. SECURITY CLASSIFICATION OF REPORT	18. SECURITY CLASSIFICATION OF THIS PAGE	19. SECURITY CLASSIFICATION OF ABSTRACT	20. LIMITATION OF ABSTRACT
Unclassified	Unclassified	Unclassified	UU

NSN 7540-01-280-5500

Standard Form 298 (Rev. 2-89)
Prescribed by ANSI Std. Z39-18
298-102

I. Objectives

The primary objective of the proposed research is to gain a fundamental understanding of strategies, mechanisms, and scaling laws for successful control of separation using zero-net mass-flux (ZNMF) actuators. Key issues that are systematically studied are optimal excitation frequencies and waveforms, pressure gradient, and curvature effects in separated flows characterized by convective and/or global instabilities. The study is a complementary experimental/numerical effort that capitalizes on previous collaborations and is aimed at leveraging the respective strengths of CFD and experiments. The computational modeling component was carried out by the George Washington University (GWU) team under the current FA9550-05-1-0169 grant, whereas the experimental component was carried out by the University of Florida (UF) team under grant FA9550-05-1-0093. The primary objectives of the computational component were the following:

1. Examine the dynamics of baseline uncontrolled flows to determine the nature of the coupling between the local instability of the separated shear layer and the global wake instability as a function of flow separation location and reattachment and curvature.
2. Investigate the effects of nondimensional forcing frequency F^+ on the associated separation control mechanisms. In particular, we seek to determine the effective frequencies for shear layer/wake forcing to capitalize on nonlinear interactions between local and global instabilities.
3. Develop scaling laws for ZNMF devices and generate data for the development and validation of lumped element models.

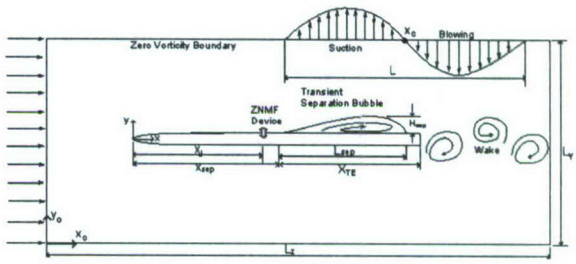

(a)

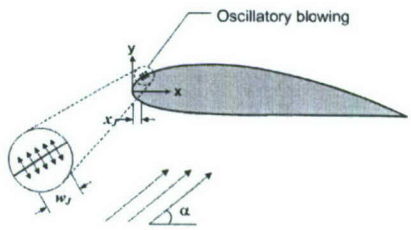

(b)

Figure 1: Schematic of the computational flow configuration employed in current study (a) Canonical separated flow (b) Separated airfoil flow

II. Status of Effort

The effort has been successful in accomplishing all of its original objectives. Below we summarize the status of the effort and provide additional details in the Section III of report.

The numerical component employed a Cartesian-grid-based incompressible DNS solver as well as unstructured grid solver developed by the Center for Turbulence Research at Stanford University (Ham & Iaccarino 2004). The Cartesian grid solver was thoroughly validated by comparing with NASA's Synthetic Jet validation database (Yao et al 2004Kotapati et al. 2007,).

The dynamics of the baseline flow have been investigated for both a canonical configuration shown in Fig. 1(a) as well as a prototypical airfoil configuration shown in Fig. 1(b). The simulations have provides new insights into the non-linear coupling between the shear layer, separation bubble and wake for separated flows. Our understanding of this non-linear coupling and lock-on phenomenon was crucial in our subsequent study of ZNMF based flow control.

The effect of the non-dimensional frequency F^+ on the separation control was also investigated thoroughly for both of the above configurations. For the canonical flow (Fig 1 a), both two-dimensional

(2D) as well as three-dimensional (3D) simulations were carried out on DoD High Performance Computing Center (HPC) platforms in order to examine the effect of this parameter as well as the associated flow physics. For the separated airfoil the study was limited to 2D simulations and we investigated the role of frequency and amplitude of forcing as well as actuator placement. The key result from these simulations was that forcing at different frequencies can move the separated flow from one-lock-on state to another and some of these new lock-on states have desirable aerodynamic characteristics whereas others are detrimental to the objective of separation control.

Numerical simulations of isolated ZNMF actuators in quiescent as well as grazing flow have been used to devise scaling laws for these actuators. In particular we focused on the pressure drop across the ZNMF slot and determined scaling laws for the relative contribution of inviscid, viscous and non-linear effects on this quantity. We also used our simulations to develop a phenomenological model for the non-linear component of pressure drop which is expected to improve the predictive capability of existing lumped-element models (Gallas 2004).

III. Accomplishments and New Findings

A. Flow Physics of a Canonical Separated Flow

A novel numerical configuration for investigating active separation control of canonical separated airfoil flows, using zero-net mass-flux (ZNMF) jets was earlier proposed by Mittal *et al* [1]. The flow configuration shown in Fig. 1 consists of a 5% thick flat plate of chord c with 8:1 elliptic leading edge and blunt trailing edge at 0° angle-of-attack in a free-stream. A separation bubble of prescribed size is induced at the aft-chord location on the upper surface of the flat plate by applying an adverse pressure gradient through blowing and suction on the upper boundary of the computational domain. The technique of Na & Moin[2] is adopted in this study, wherein a zero-vorticity boundary condition of the following form is prescribed on the upper boundary:

$$v(x_0, L_y) = G(x_0), \qquad \left.\frac{\partial u}{\partial y_0}\right|_{(x_0, L_y)} = \frac{dG}{dx_0}, \tag{1}$$

where $G(x_0)$ is the prescribed blowing and suction velocity profile, and the Neumann boundary condition on u ensures that no spanwise vorticity is generated due to blowing and suction. The function $G(x_0)$ allows us to prescribe the location as well as the streamwise size of the separation region. The advantages of using such a configuration are explained in detail in the work of Kotapati *et al* (2006).

The flow field is obtained using CDP, an unstructured grid finite-volume based flow solver developed at the Center for Turbulence Research, Stanford University (Ham & Iaccarino 2004). First, the uncontrolled version of the flow configuration with aft-chord separation is simulated to determine the characteristic frequency scales: f_{SL}, f_{sep}, and f_{wake}. Aft-chord separation is induced by prescribing blowing and suction over $0.7 \le x/c \le 1.3$ on the top boundary of the computational domain. The characteristic frequencies are determined by computing power spectra of time-series of v-velocity in the shear layer, the separated region, and the wake. Simulations are then carried out with ZNMF perturbation of the boundary layer at various subharmonics and superharmonics of the characteristic frequencies.

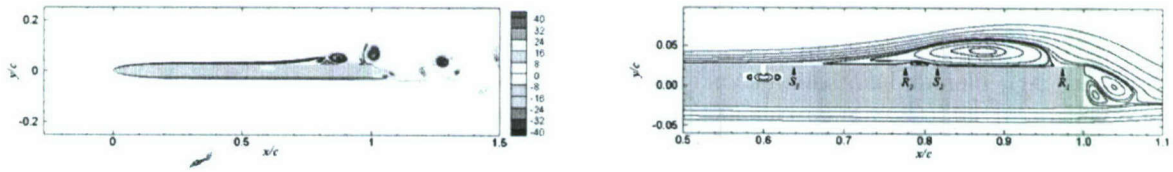

Figure 3: Instantaneous spanwise vorticity and mean streamlines for the baseline separated flow.

Figure 3 shows the contours of instantaneous spanwise vorticity and mean streamline pattern obtained for the baseline uncontrolled flow (Case 0). The boundary layer separates at $x/c = 0.646$ and the separated shear layer directly rolls up into large Kelvin–Helmholtz (KH) type vortices without any subharmonic pairing. When these large vortices are of some appropriate size and strength, they pinch off from the shear layer and convect downstream into the wake. This yields a closed aft-chord separation bubble in the mean with distinct primary separation and reattachment points, S_1 and R_1, respectively. The mean separation bubble also contains secondary separation S_2 and reattachment R_2 of the reverse flow induced by the roll-up of large vortices. The length L_{sep} and the height H_{sep} of the mean separation bubble measure $0.308c$ and $0.029c$, respectively.

Table 1: Various cases considered in the current study.

Case	0	1	2	3	4	5	6	7	8
$F^+ = fc/U_\infty$	No forcing	0.725	0.97	1.45	2.9	3.625	5.8	8.7	11.6

The power spectra corresponding to the temporal variations of cross-stream velocity v for Case 0 in the shear layer, the separation zone, and the wake, respectively, shown in Fig. 4(a) indicate that the shear layer, the separation zone, and the wake are all locked on to a single frequency fc/U_∞ of around 2.9. We now examine the effect of forcing the ZNMF jet slightly upstream of the point of separation at the lock-on frequency and its harmonics as shown in table 1. Figure 5 shows contours of instantaneous spanwise vorticity and mean streamlines, respectively, for Cases 1–8. It is clear that forcing the shear layer at a frequency that is somewhere in between the lock-on frequency or its first superharmonic immediately reattaches the shear layer to the airfoil surface and delays separation farther downstream, besides reducing the height of the separation bubble significantly.

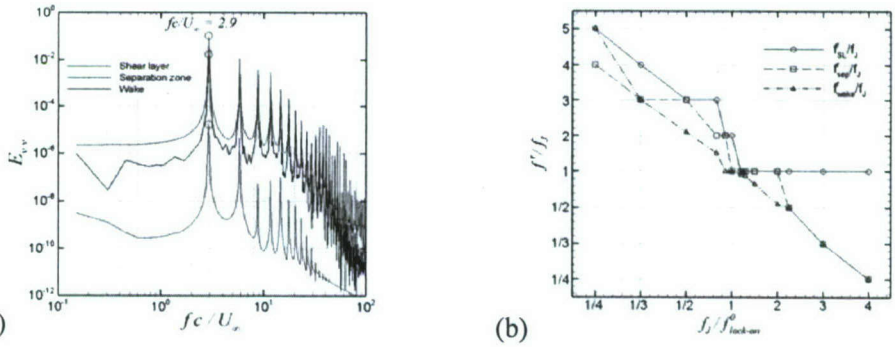

Figure 4: (a) Power spectra corresponding to cross-stream velocity in the shear layer, separation region and wake for the baseline separated flow. (b) Lock-on map of the response at various forcing frequencies

The lock-on map in Fig. 3(b) summarizes the frequency response to forcing for Cases 1–8. Forcing at subharmonics (Cases 1–3) of the lock-on frequency causes the shear layer to lock on to the superharmonics of the forcing frequency, whereas forcing the shear layer at the lock-on frequency and its superharmonics causes it to resonate with the forcing frequency. However, when the shear layer is forced at a frequency that is somewhere in between the lock-on frequency or its first superharmonic (Case 5), the entire system changes its state and locks on to the forcing frequency. As discussed by Wu *et al* (1998) such as frequency lock-in due to forcing leads to a more regularized flow than the non-resonant case, thereby resulting in effective separation control. In the proximity of such a lock-in region, the separation bubble is found to effectively couple with the shear layer over a wider bandwidth than the wake and the wake does not influence the dynamics of the separation bubble. However, farther outside of this region, the wake appears to have significant influence over the separation bubble because of its global instability. Forcing the shear layer at higher superharmonics appears to amplify K–H type instabilities in the separated shear layer leading to roll-up and subharmonic pairing in the separated region. As shown by the

mean streamlines, this process further deteriorates the separated region rendering ZNMF forcing ineffective.

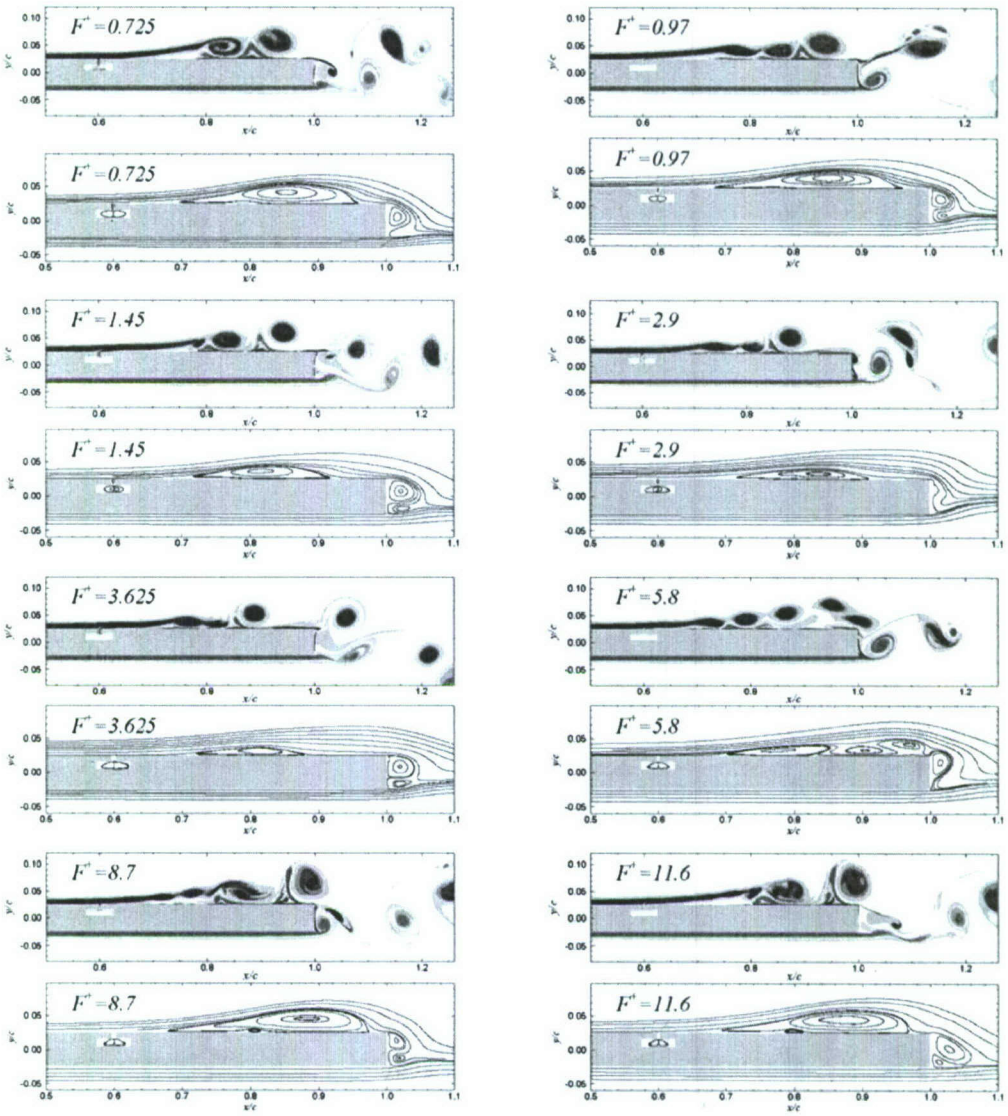

Figure 5: Instantaneous spanwise vorticity and mean streamlines for cases with forcing at different frequencies.

B. Airfoil Separation Control using ZNMF periodic excitation

A parametric approach similar to the one used for the canonical separated flow is extended to separated flow over a conventional airfoil. The aim is here to examine the detailed flow physics over a stalled airfoil and its response to the different forcing frequencies. For this purpose 2-D NACA 4418 airfoil is chosen as seen in Fig. 5. Experiments of Zaman & Culley (2006) have examined the effects of frequencies and velocity amplitude at a single jet location for post-stall cases at high α. For the present work however we have chosen a post-stall case at a moderately high α =18° where the separated flow shows reattachment. Thus it is expected that this flow will contain all three naturally occurring frequencies. Forcing is examined for 2D simulations carried out at Re_c =40,000 and α =18°, on a

structured grid with 384 × 157 grid points. An oscillatory boundary condition on the airfoil surface at a distance x_J / c from the leading edge of the form $V_0 \sin(2\pi f_J t)$ is used to model the ZNMF actuator.

The baseline uncontrolled cases are compared with the experimental results as seen in Fig. 6(a-b). The drag data show a reasonable match with the experimental data while the lift reflects the onset of stall around $\alpha = 17^\circ$ for the present conditions similar to high Re_c conditions (Abbot and Doenhoff 1959) The time-averaged streamlines seen in Fig. 6(c) show that the flow separates at a distance $x/c = 0.032$ from the leading edge and reattaches in the mean showing primary and secondary recirculation regions. The natural frequencies of the flow can be characterized by looking at the temporal variations of the cross-stream and its corresponding power spectra shown in Fig. 6(d-e). The frequencies are found to be $f^+_{wake} = 1, f^+_{sep} = 2.25$ and $f^+_{wake} = 11.75$ for the wake, separation bubble and shear layer respectively. The forcing frequencies for control cases are chosen to cover the range these natural frequencies as $f^+_J = 0.5$ to 12, while $V_0 = 0.1U_\infty$, $x_J / c =$ 0.024 and $l_c =$ 0.012. In addition one case with $f^+_J = f^+_{sep}$ and $x_J / c =$ 0.070 is also chosen, such that forcing takes place inside the separation bubble.

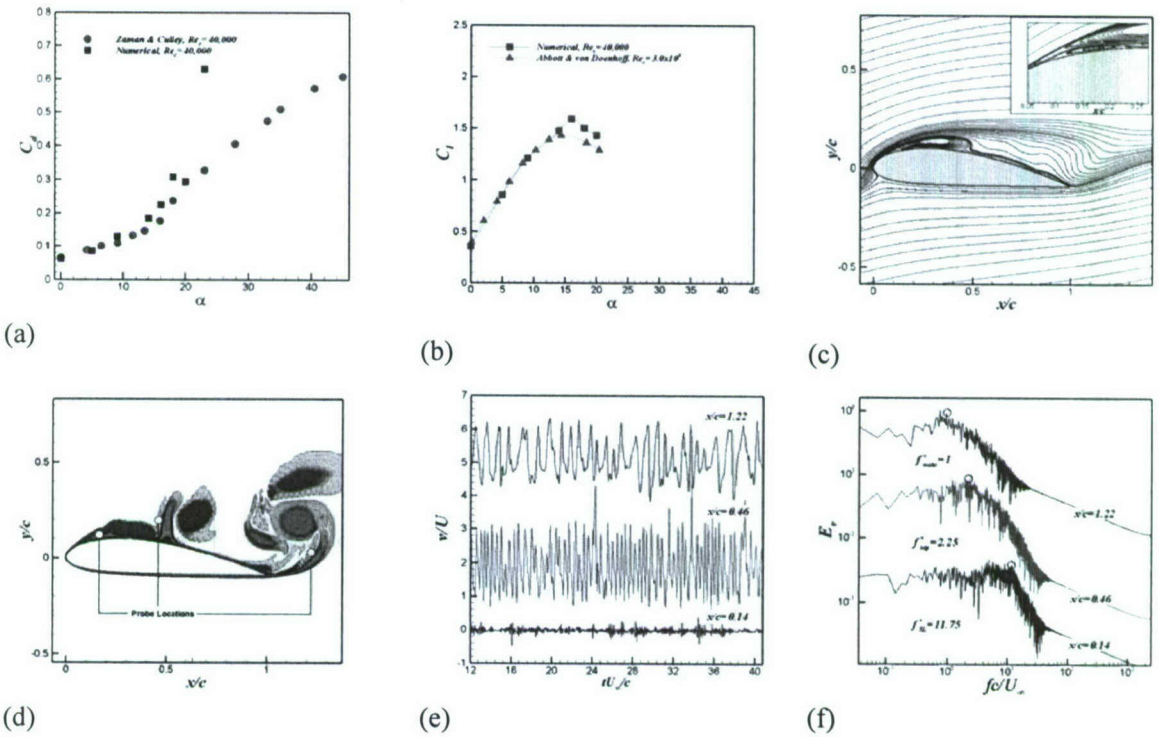

Figure 6: Simulation results for the airfoil showing, (a) comparison of drag and (b) lift at various angles of attacks with experimental data[6,7], (c) time-averaged mean streamlines, (d) instantaneous vorticity counters showing probe locations. The corresponding (e) temporal variation of cross-stream velocity and (f) its spectra.

Fig. 7(a-c) show the instantaneous spanwise for select cases which reflect that forcing at frequencies near f^+_{sep} produces discrete vortices which are convected downstream traveling close to the airfoil surface, however for $f^+_J = 0.5$ and higher frequencies larger vortices are formed due to longer time scales for the former and rolling up coalescence of the shear layer for the latter. This is reflected in the separation bubble characteristics where forcing frequencies based on or near the separation bubble frequency tends to reduce the separation considerably while the latter two cases tend to increase the separation as seen in Fig. 7(d-e).

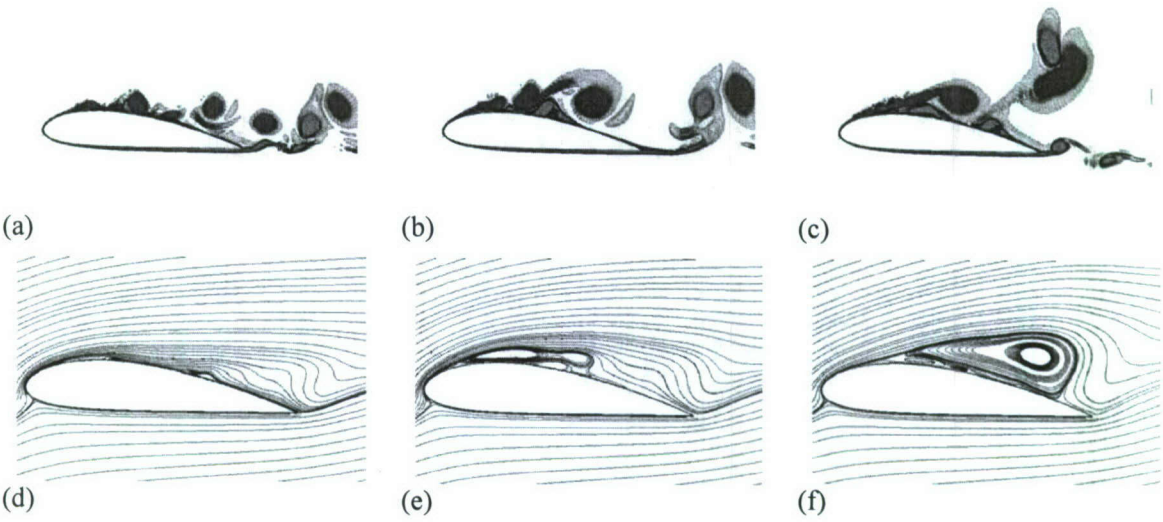

Figure 7: Instantaneous spanwise vorticity for (a) $f_J^+ = 2$, (b) $f_J^+ = 0.5$ and (c) $f_J^+ = 12$ at ; time averaged mean streamlines showing primary separation regions (d) $f_J^+ = 2$, (e) $f_J^+ = 0.5$ and (f) $f_J^+ = 12$.

Fig. 8(a) compares the drag coefficients with forcing to the baseline case. It is found that frequencies closer to the f_{sep}^+ show significant reduction in the drag with $f_J^+ = 2$, $x_J^+ = 0.024$ case showing approximately 37% decrease with the exception of forcing at $f_J^+ = 0.5$ & x_J^+=$ 0.024 which increases the drag by 12%. On the other hand operating at higher forcing frequencies increases the drag by nearly 25-42%. However unlike the drag there in no significant variation in the lift component seen in Fig. 8(b). Comparison of the lift-to-drag ratio in Fig. 8(c) shows overall improvement in this quantity by nearly 60% for $f_J^+ = 2$ & $x_J^+ = 0.024$ while the higher frequency cases show a decrease up to 35% in the lift-to-drag ratio.

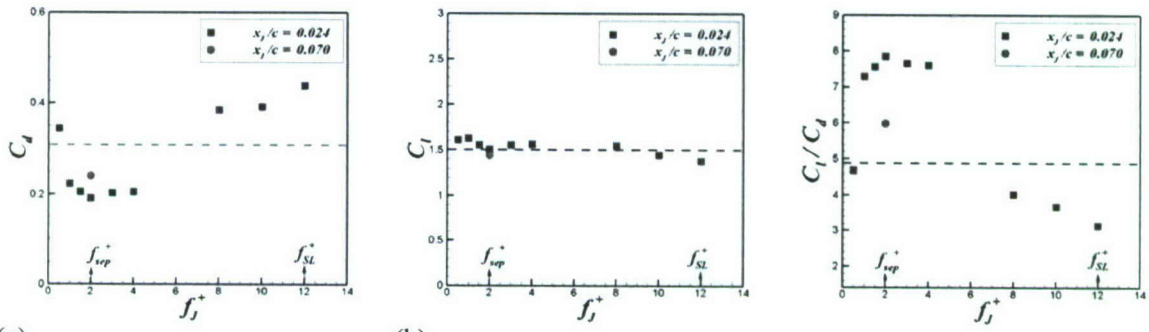

Figure 8: Comparison of aerodynamics characteristics for different forcing frequencies showing (a) drag coefficient, (b) lift coefficient and (c) lift to drag ratio. Dashed line indicate baseline uncontrolled values.

C. Scaling of Pressure Drop across the orifice of a ZNMF device

The development of reduced order models like the lumped element model require the quantitative understanding of unsteady flow physics inside the orifice of a ZNMF device. For example, the presence of entrance and exit "minor" losses across the slot, which cause a nonlinear drop in pressure, need to be accounted for in the lower order models.(Gallas et al 2004) Pressure drop across the orifice is difficult to

compute experimentally and analytical models are required to predict the same. Using the control volume analysis for an incompressible, laminar flow in a non-deformable slot (control volume shown in Fig. 9) an analogy for oscillatory flow can be derived from steady flows (White 1991) to obtain the relation for the pressure drop across slot length, h as

$$\Delta C_p = \underbrace{\int_0^{x/d} C_f \, d\left(\frac{x}{d}\right)}_{\Delta C_{p-shear}} + \underbrace{\frac{x}{d}\pi St\cos(\omega t)}_{\Delta C_{p-unsteady}} + \underbrace{2\int_{-1/2}^{1/2}\left(\frac{u_x^2 - u_0^2}{\bar{U}_j^2}\right) d\left(\frac{y}{d}\right)}_{\Delta C_{p-mom}} \qquad (2)$$

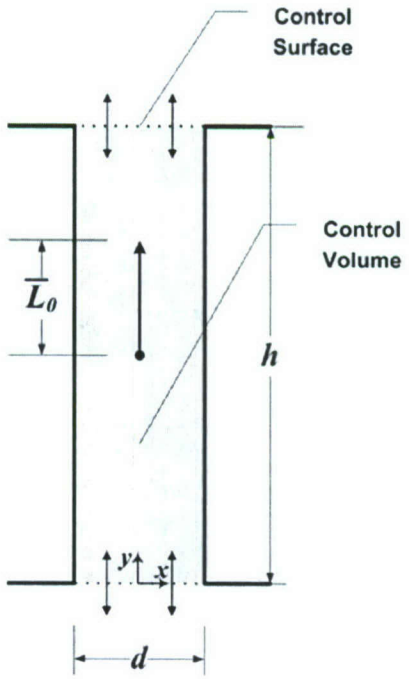

Figure 9 Schematic of the 2D control volume used for the analysis.

The terms on the RHS of Eq. (2) are viscous shear stress contribution to the pressure drop ($\Delta C_{p-shear}$), unsteady inertia term ($\Delta C_{p-unsteady}$) and nonlinear pressure drop to accelerate flow (ΔC_{p-mom}). In order to validate this analysis both experiments and numerical simulations have been performed. The control volume analysis is able to give an informative breakdown of the pressure drop in terms of individual components. However the goal is to be able to present a simplified model which can predict the individual term based on the governing parameters. For this reason simple scaling arguments are used to analyze this dependence. A key parameter in the current study is the average "stroke" length $\overline{L_0}$ which is defined as $\overline{L_0} = (1/S_n)\int_0^{T/2} Q(t)dt$ where $Q(t)$ is the volume flow rate through the orifice area S_n. Eq. (2) shows that the unsteady term is governed by two dimensionless parameters St and h/d by which it can be scaled since

$$\Delta C_{p-unsteady} = \pi St.\frac{h}{d}\cos(\omega t) \propto St.\frac{h}{d} \qquad (3)$$

The root mean square (rms) contribution of each term plotted versus $(St.h/d)$ confirmed the scaling for this term. It also shows that for higher values of $(St.h/d)$, the unsteady term is dominant, while for values around unity and below, the contributions of both the momentum and unsteady terms become comparable. While the trend of the unsteady term was clear, the scaling of the remaining terms on the RHS of (2) is not apparent in this plot. Dimensional analysis of each term is used to gain an insight to the scaling. The viscous contribution to the pressure drop is proportional to the shear term integrated over the normalized slot length – i.e.

$$\Delta C_{p-shear} = \int_0^{h/d} C_f d\left(\frac{y}{d}\right) \propto C_f \frac{h}{d} = \frac{\tau_w}{0.5\rho \overline{V_J}^2} \frac{h}{d} \tag{4}$$

If we assume that the appropriate length scale for boundary layer in the slot is the Stokes layer viscous length scale $\sqrt{\upsilon/\omega}$ (White 1991), while $\overline{V_J}$ is the appropriate velocity scale, dimensional analysis then yields

$$\Delta C_{p-shear} \approx \mu \frac{\partial u}{\partial y} \frac{h}{d} \frac{1}{0.5\rho \overline{V_J}^2} \approx \mu \frac{\overline{V_J}}{\sqrt{\upsilon/\omega}} \frac{h}{d} \frac{1}{\rho \overline{V_J}^2} = \frac{(h/d).S}{\mathrm{Re}_J} \tag{5}$$

Figure 10 shows a plot of the rms values of the $\Delta C_{p-shear}$ calculated from the numerical simulations plotted against $(h/d).S/\mathrm{Re}_J$. A linear best-fit line through the data shows a relative rms error of approximately 10%. As was seen for Cases 1 – 4, with low Re_J the contribution of $\Delta C_{p-shear}$ is more significant than the nonlinear term and hence we obtain a fairly accurate linear model for predicting these viscous losses.

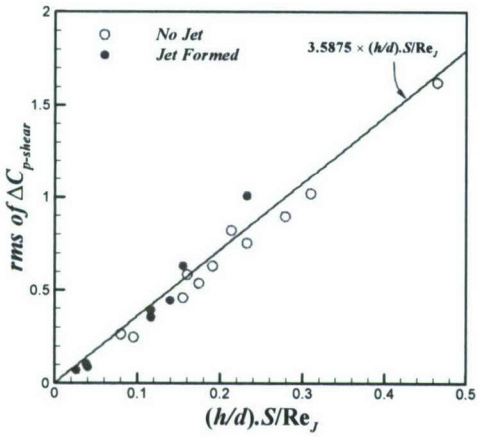

Figure 10: rms values of $\Delta C_{p\text{-}shear}$ as function of $(h/d)\cdot S/\mathrm{Re}_J$.

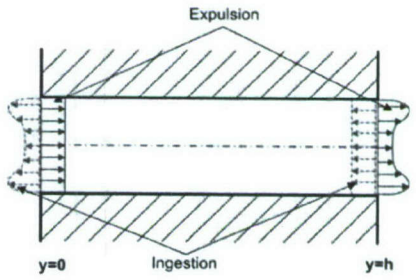

Figure 11: Schematic showing the velocity profile assumed for the phenomenological model.

The final term that remains to be accounted for is the ΔC_{p-mom} term, which is usually expressed as the nonlinear loss coefficient, K_d based on $\overline{V_J}$ in LEM (Gallas et al. 2003). This coefficient can be related to the nonlinear momentum term as

$$K_d = \left(\frac{2}{\pi}\right)^2 \Delta C_{p-mom} \tag{6}$$

Due to its nonlinear nature, this term is particularly difficult to scale or model. Interestingly, the simulations indicate that when $\overline{L_0}/h >> 1$ the slot flow profile is simpler than when $\overline{L_0}/h << 1$ when no jet is formed. This is because for these cases where a clear jet is formed, the local flow field near the lips of the orifice are not affected by secondary vortices. This suggests that simple descriptions of the slot flow might suffice to parameterize the nonlinear pressure drop for these flows.

Here we propose a phenomenological model which assumes that during expulsion the inlet flow at $y = 0$ has a uniform plug flow velocity sinusoidal in time, $V_{plug}(t)$. While at the exit ($y = h$) the flow has a fully developed oscillatory flow profile given by

$$v_{x=h}(y, 0 \le \omega t \le \pi) = \frac{V_{amp}}{i\omega\rho}\left[1 - \frac{\cosh\left[S\sqrt{i}\, y/d\right]}{\cosh\left[S\sqrt{i}/2\right]}\right] e^{i\omega t} \tag{7}$$

where V_{amp} is a constant governing the velocity amplitude, and the continuity equation is used to ensure that the inlet and exit profiles are in phase. This is based on the solution of the fully developed oscillatory flow in a channel given by Loudon & Tordesillas (1999). The schematic of flow conditions for this model is presented in Figure . As indicated in Figure , it is assumed that the situation reverses during the flow ingestion phase, i.e., at $y = h$ there is a uniform plug profile. Based on these assumptions the nonlinear momentum term ΔC_{p-mom} in Eq. (2) can be approximated as,

$$\Delta C_{p-mom} = 2\int_{-1/2}^{1/2} \frac{v_h|v_h| - V_{plug}|V_{plug}|}{\overline{V_J}^2} d\left(\frac{y}{d}\right) \tag{8}$$

and substitution of the real part of Eq. (7) in this integral provides a prediction of ΔC_{p-mom}. Within the framework of this model, the ΔC_{p-mom} term and hence, K_d is a function only of the Stokes number S. This is due to the normalization of the momentum term which eliminates the V_{amp} term governing the jet Reynolds number, Re_J.

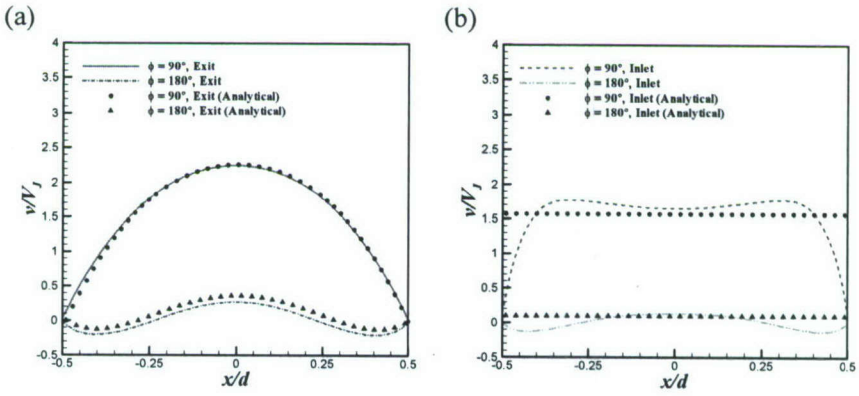

Figure 12 Comparison of the proposed analytical and computed phase-averaged v-velocity for Re_J=54, S=5, h/d=2.5 (Case-1) at the slot (a) exit and (b) inlet.

The proposed phenomenological model is compared with some of the numerical simulations to assess its fidelity. Fig. 12 shows the results for the proposed model at S=5 compared with Case-1, Re_J=54, S=5 and h/d=2.5. At the exit plane the proposed model is able match the velocity profile seen in Fig 12(a). On the other hand Fig. 12(b) shows that the plug profile at the inlet phase is able to give an approximation of the velocity amplitude only. Interestingly the exit profile indicates that the flow is fully developed even for $\overline{L_0}/h$=2.71 which can be attributed to the low Re_J for this case. Hence comparison with the phenomenological model also serves as a means of determining whether or not the flow is fully developed. For the current simulations it was found that for $\mathrm{Re}_J > 100$ and $\overline{L_0}/h >> 1$ the flow is not fully developed. This is clear from Fig 13 where for Case-3 conditions of Re_J=262, S=10 and h/d=0.68 ($\overline{L_0}/h$=2.10) the flow is not fully developed. However, the proposed model does give a reasonable approximation to velocity profiles.

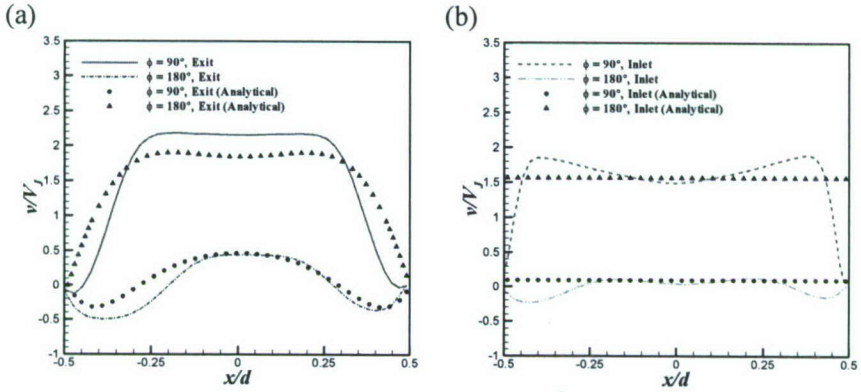

Figure 13: Comparison of the proposed analytical and computed phase-averaged v-velocity for Re_J=262, S=10, h/d=0.68 (Case-11) at the slot (a) e and (b) inlet.

The computed ΔC_{p-mom} term for the aforementioned cases is compared with the analytical model in Fig. 14. It can be seen that the model over-predicts the magnitude of this term for S=5 when compared to Case-1 while capturing the trend of its variation over a cycle. However for Case-3 seen in 14(b) it is unable to capture the peak during maximum expulsion.

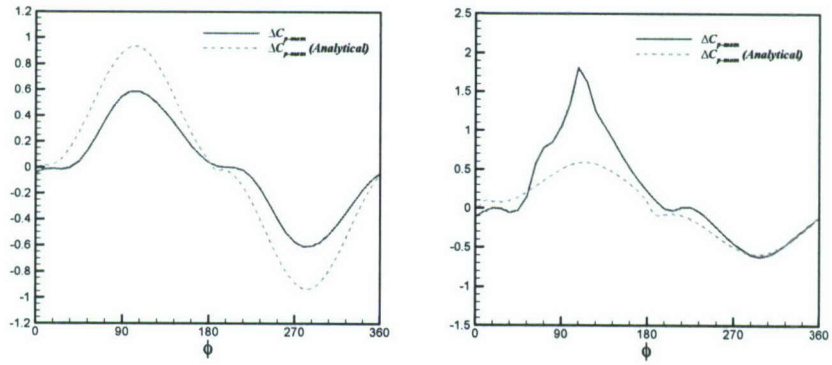

Figure 14: Comparison of the proposed analytical and computed ΔC_{p-mom} over a cycle for (a) Case-1 and (b) Case-2.

Based on the rms of ΔC_{p-mom} the loss coefficient K_d is plotted in Figure versus S as estimated from the model as well as the values obtained from the simulations. A number of interesting observations can be made regarding this plot. First, as $S \to 0$ the flow becomes quasi-steady, and the rms loss coefficient asymptotes to the equivalent steady value of 0.245 (see section 4-9 in White [1991]). Furthermore, the phenomenological model seems to provide a reasonable prediction of the magnitudes and trend (generally decreasing with increasing S and approaching 0 as $S \to \infty$). Note that current LEM (Gallas *et al.* [2003]) usually employ a constant value of unity, which is equivalent to $(2/\pi)^2/\sqrt{2} = 0.286$ in the current rms normalized values, to account for both nonlinear and viscous losses. The datum from Case-19 is significantly higher forming an outlier for the proposed model and hence has not been presented here. From the computational data set of the reaming 18 cases, we find that the rms error (normalized by the steady-state value of 0.245) is reduced from 0.69 for the current LEM to 0.29 for the proposed model. Thus, the simple phenomenological model proposed here, although based only on S, is able to provide a significantly better estimate of the loss coefficient and can therefore be used to increase the accuracy of existing LEM.

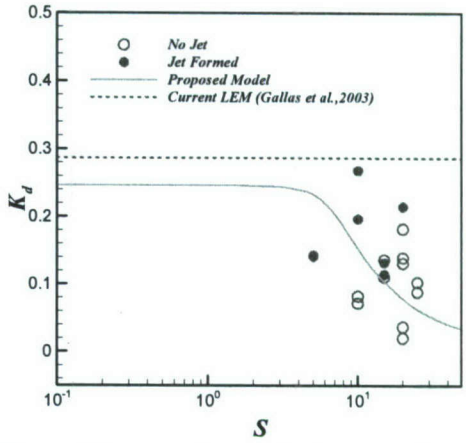

Figure 15: rms value of the loss coefficient K_d versus Stokes number S.

Publications Resulting From Grant

- Raju, R., Gallas, Q., Mittal, R. and Cattafesta, L., "Scaling of Pressure Drop across a Slot with Oscillatory Flows", *Physics of Fluids* Vol. 19, 078107, 2007.
- Kotapati, R. B., Mittal, R and Cattafesta, L.N, "Numerical study of a transitional synthetic jet in quiescent external flow" *Journal of Fluid Mechanics*, 581, June 2007 pp 287-321.
- Raju, R., Mittal, R. and Cattafesta, L.N, "Towards Physics Based Strategies for Separation Control over an Airfoil using Synthetic Jets " 45th AIAA Aerospace Sciences Meeting and Exhibit, Reno, Nevada, AIAA Paper 2007-1421.
- Raju, R., Mittal, R., Marxen, O., Ham, F. and You, D., "Numerical Simulations of Synthetic Jet Based Separation Control in a Canonical Separated Flow" 45th AIAA Aerospace Sciences Meeting and Exhibit, Reno, Nevada, AIAA Paper 2007-1308.
- Kotapati, R. B., Mittal, R and Cattafesta, L.N, "Numerical Experiments in Synthetic Jet Based Separation Control", AIAA Paper 2006-0320, January 2006.
- Tian, Y., Cattafesta, L. and Mittal, R. "Adaptive Control of Separated Flow," AIAA Paper 2006-1401, 2006.
- Holman, R. Y. Utturkar, R. Mittal, B. Smith and L. N. Cattafesta III "A Jet Formation Criterion for Synthetic Jets," *AIAA Journal*, Vol.43, No.10, October 2005.
- Mittal, R., Iaccarino, G., "Immersed Boundary Methods," *Annual Review of Fluid Mechanics*, Vol. 37, pp.239-261, 2005.
- Raju, R. R. Mittal, Q. Gallas, and L. N, Cattafesta III "Scaling of Vorticity Flux and Entrance Length effects in Zero-Net Mass-Flux Devices,", AIAA Paper 2005-4751, June 2005.
- R. B. Kotapati, and R. Mittal "Time-Accurate Three-Dimensional Simulations of Synthetic Jets in

Quiescent Air,", AIAA Paper 2005-0103, January 2005.

- R. Mittal, R. B. Kotapati and L. N. Cattafesta III "Numerical Study of Resonant Interactions and Flow Control in a Canonical Separated Flow,", AIAA Paper 2005-1261, January 2005.
- R. Mittal and R. B. Kotapati "Resonant Mode Interaction in a Canonical Separated Flow," *IUTAM Symposium on Laminar-Turbulent Transition*, December 2004, Bangalore, India.

Theses/Dissertations Associated with Grant

1. "Scaling Laws and Separation Control Strategies for Zero-Net Mass-Flux Actuators" by Reni Raju, D.Sc. Dissertation. George Washington University, December 2007.
2. "A Numerical Study of Three Dimensional Synthetic Jets in Quiescent and External Grazing Flows" by Ravi Byrganhalli, D.Sc. Dissertation. George Washington University, May 2007.
3. "On Synthetic Jets and Their Application to Separation Control in Canonical Airfoil Flows." D.Sc. dissertation, Mechanical and Aerospace Engineering, The George Washington University, Washington, October 2007.

Honors & Awards Received

Rajat Mittal received the 2006 Lewis B. Moody Award from ASME.

Personnel Supported

Reni Raju	Doctoral Student, The George Washington University
Rupesh B. Kotapati	Doctoral Student, The George Washington University
Ravi Byrganhalli	Doctoral Student, The George Washington University
Haibo Dong	Postdoctoral Research Scientist, The George Washington University
Rajat Mittal	Professor, The George Washington University

Bibliography

1. Abbott, I. H. and von Doenhoff, A. E., *Theory of Wing Sections Including a Summary of Airfoil Data* (Dover Publications Inc., New York, 1959).
2. Gallas, Q., Holman, R., Nishida, T., Caroll, B., Sheplak, M. and Cattafesta, L., "Lumped Element modeling of Piezoelectric-Driven Synthetic Jet Actuators," *AIAA Journal*, Vol. 41, No. 2, pp. 240-247, 2003.
3. Gallas, Q., Holman, R., Raju, R., Mittal, R, Sheplak, M., and Cattafesta, L., "Low Dimensional Modeling of Zero-Net Mass-Flux Actuators," *AIAA* 2004-2413, 2004.
4. Ham, F. & Iaccarino, G. 2004 Energy conservation in collocated discretization schemes on unstructured meshes, Tech. Rep., Center for Turbulence Research (CTR) Annual Research Briefs.
5. Kotapati, R.B., Mittal R. and Cattafesta, L., "Numerical Experiments in Synthetic Jet Based Separation Control" AIAA Paper 2006-0320, 2006.
6. Loudon, C. and Tordesillas, A. "The use of the dimensionless Womersley number to characterize the unsteady nature of internal flow," *Journal of Theoretical Biology*, Vol.191, pp. 63-78, 1998.
7. Mittal, R., Kotapati, R.B., and Cattafesta III, L.N. "Numerical Study of Resonant Interactions and Flow Control in a Canonical Seperated Flow," AIAA 2005-1261, 2005.

8. Na, Y. & Moin, P. 1998 Direct numerical simulation of a separated turbulent boundary layer, *J. Fluid Mech.*, 370,175–201.

9. White, F.M., *Viscous Fluid Flow* (McGraw-Hill, Inc., New York, NY, 2nd ed., 1991.

10. Wu, J. -Z., Lu, X. -Y., Denny, A. G., Fan, M. & Wu, J. -M. 1998 Post-stall flow control on an airfoil by local unsteady forcing, *J. Fluid Mech.*, 371, 21–58.

11. Yao, C. S., Chen, F. J., Neuhart, D., and Harris, J., "Synthetic Jets in Quiescent Air," *Proc. NASA LaRC Workshop on CFD Validation of Synthetic Jets and Turbulent Separation Control*, Williamsburg, Virginia, March 29-31, 2004.

12. Zaman, K.B.M.Q and Culley, D.E., "A study of Stall control over an Airfoil using 'Synthetic Jets'," AIAA Paper 2006-98, 2006.